Published in final edited form as:

Dev Biol. 2021 April ; 472: 18–29. doi:10.1016/j.ydbio.2020.12.020.

Multiple roles for *Pax2* in the embryonic mouse eye

Bernadett Bosze[1], **Julissa Suarez-Navarro**[1], **Abdul Soofi**[2], **James D. Lauderdale**[3], **Gregory R. Dressler**[2], **Nadean L. Brown**[1,*]

[1]Department of Cell Biology & Human Anatomy, University of California Davis, One Shields Avenue, Davis, CA 95616 USA

[2]Department of Pathology, University of Michigan School of Medicine, Ann Arbor, MI 48109 USA

[3]Department of Cellular Biology, University of Georgia, Athens, GA 30602

Abstract

The vertebrate eye anlage grows out of the brain and folds into bilayered optic cups. The eye is patterned along multiple axes, precisely controlled by genetic programs, to delineate neural retina, pigment epithelium, and optic stalk tissues. Pax genes encode developmental regulators of key morphogenetic events, with *Pax2* being essential for interpreting inductive signals, including in the eye. *PAX2* mutations cause ocular coloboma, when the ventral optic fissure fails to close. Previous studies established that *Pax2* is necessary for fissure closure and to maintain the neural retina -- glial optic stalk boundary. Using a $Pax2^{GFP/+}$ knock-in allele we discovered that the mutant optic nerve head (ONH) lacks molecular boundaries with the retina and RPE, rendering the ONH larger than normal. This was preceded by ventronasal cup mispatterning, a burst of overproliferation and followed by optic cup apoptosis. Our findings support the hypothesis that ONH cells are tripotential, requiring *Pax2* to remain committed to glial fates. This work extends current models of ocular development, contributes to broader understanding of tissue boundary formation and informs the underlying mechanisms of human coloboma.

Keywords

Pax2; Pax6; Foxg1; retina; RPE; optic stalk; coloboma

INTRODUCTION

Mouse eye formation begins with specification of the embryonic eye field within the anterior neural plate, followed by bilateral optic vesicle outgrowth from the ventral diencephalon (reviewed in Fuhrmann, 2010; Martinez-Morales et al., 2017). Upon reaching the surface ectoderm, a set of stereotypical morphologic movements transforms the optic vesicle into a cup. One important hallmark of optic vesicle invagination is the appearance of an optic (or

*Author for correspondence (nlbrown@ucdavis.edu).

choroid) fissure, the transient groove along the ventral side of the developing eye and optic stalk. The edges of this fissure progressively fuse together, with complete closure at E12.5. Simultaneously, a collar of cells, termed the optic nerve head (ONH) or optic disc, arise at the interface of the optic cup and stalk. The ONH is an important structure in the developing eye, because it is comprised of lineage-restricted cells that serve as a boundary between the neural retina and glial optic stalk (reviewed in Tao and Zhang, 2014). Moreover, the opening at the back of the eye, encircled by the ONH, is both an exit for retinal ganglion cell (RGC) axons connecting to the brain, and entrance for blood vessels that support the adult retina.

Failed optic fissure closure (coloboma) and/or abnormal ONH formation arise in a variety of congenital diseases, resulting in visual impairment or blindness (reviewed in ALSomiry et al., 2019). Our understanding of coloboma at the molecular level remains incomplete, with the genetic hierarchy regulating optic fissure closure only partially known. A myriad of signaling pathways play essential roles in the coloboma network. For example, midline-derived *Shh* signaling is one of the earliest factors for establishing proximal-distal and dorsal-ventral coordinates in the optic vesicle. *Shh* activity also regulates the expression of multiple *Pax* genes, a protein family primarily characterized by a paired-box DNA binding motif (reviewed in Blake and Ziman, 2014; Bopp et al., 1986). Both *Pax2* and *Pax6* are required at multiple stages of vertebrate eye development (reviewed in Kozmik, 2005). *Pax6* expression initiates within the eye field and is present in every ocular tissue at particular developmental stages (Shaham et al., 2012). Human *PAX6* mutations are associated with multiple ocular syndromes, including MAC (Microphthalmia/Anophthalmia/Coloboma), Aniridia and Peter's anomaly (reviewed in Prosser and van Heyningen, 1998; Tzoulaki et al., 2005). *Pax2* is initially expressed uniformly within the optic vesicle (Lee et al., 2005; Nornes et al., 1990; Schwarz et al., 2000), but subsequently becomes localized to the proximo-ventral cup and stalk; then further refined to the ONH and optic stalk cells that adopt glial fates (Soukkarieh et al., 2007). *PAX2* human mutations, consistent with its multiple expression domains, are linked to 14 different syndromes, with isolated or combinatorial malformations of renal, auditory and visual systems (reviewed in Amiel et al., 2000). Human *PAX2* and *PAX6* mutations are haploinsufficient in the visual system, meaning one mutant copy is sufficient to induce malformations, with homozygosity incompatible with viability (Sanyanusin et al., 1995; Sisodiya et al., 2001).

Pax2 mutations have also been identified in fruit fly, zebrafish and mouse model organisms, each exhibiting eye defects (Brand et al., 1996; Favor et al., 1996; Fu and Noll, 1997; Keller et al., 1994; Otteson et al., 1998; Sanyanusin et al., 1995; Torres et al., 1996). There is deep conservation of the entire *Pax* gene family, but this is particularly true for *Pax6* and *Pax2* and the visual system. In mice, there are different types of *Pax2* mutations, including a germline targeted allele (Torres et al., 1995), ENU-induced point mutations (Cross et al., 2011) and the *Krd* 7cM deletion (Keller et al., 1994; Otteson et al., 1998). Homozygous *Pax2* mutants have urogenital, brain, ear and eye deformities, and are non-viable at birth. In the embryonic eye, both retinal and RPE tissues abnormally extend into the optic stalk, contributing to failed optic fissure closure, and bilateral coloboma (Schwarz et al., 2000). Thus, *Pax2* both delineates and maintains the optic cup-stalk boundary. In the optic vesicle, the Pax6 and Pax2 domains are initially coincident, but become progressively restricted to abut one another by E13.5, driven in part by cross-repression of each other's transcription (Schwarz et

al., 2000). An important consequence of disrupting this boundary is aberrant RGC axon guidance (Torres et al., 1996).

Here, we took advantage of a *Pax2*$^{GFP/+}$mouse, which harbors a GFP knock-in allele that abolishes *Pax2* function and expresses an EGFP reporter (*Pax2*^{GFP}). Although urogenital and auditory phenotypes of this *Pax2*^{GFP} allele have been characterized (Ranghini and Dressler, 2015; Schaefer et al., 2018; Soofi et al., 2012), nothing is known about its ocular expression and developmental defects. There are multiple unresolved questions about the roles of *Pax2* in the mammalian eye, which have been hampered in part by the lack of a *Pax2* live reporter mouse. In this paper, we demonstrate that *Pax2*$^{GFP/+}$ expression is a reliable proxy for endogenous *Pax2* expression and found no *Pax2*$^{GFP/+}$ eye phenotypes ($n \geq 50$ litters between E11-E16). However, *Pax2*$^{GFP/GFP}$ embryos have optic fissure closure defects, and effectively lack an ONH neural-glial boundary. Unexpectedly, we discovered that the GFP domain in *Pax2*$^{GFP/GFP}$ optic cups is greatly expanded. This correlated with cell autonomous overproliferation at E11.5, followed by apoptosis at E16.5, particularly of nascent RGCs. Our data are also consistent with *Pax2* acting downstream of *Foxg1* during optic fissure closure (Smith et al., 2017). The ability to visualize the *Pax2* mutant lineage here highlighted the tripotential of ONH cells (neural, RPE, glial), with *Pax2* normally directing them to glial fates. This study provides better understanding of the cellular and molecular events that contribute to ocular coloboma.

RESULTS

Pax2$^{GFP/+}$ reporter expression and *Pax2*$^{GFP/GFP}$ ocular phenotypes

The *Pax2*^{GFP} knock-in reporter is visible in living mouse embryos, initially within the anterior neural plate, including presumptive eye field cells (Fig. 1A), accurately reflecting endogenous *Pax2* expression (Nornes et al., 1990; Torres et al., 1996). At E9.5, EGFP expression is evident in the forming optic vesicles, otic vesicles, midbrain-hindbrain boundary (MHB) and developing kidneys, also mirroring endogenous *Pax2* domains (Fig. 1B). In the E11.5 eye, EGFP fluorescence is localized to the ventral optic cup, along the optic fissure (Fig. 1C,C'). Pax2 expression is downregulated as the fissure closes, and by E13.5, antibody co-labeling of cryosections showed high correlation of cytoplasmic EGFP and nuclear Pax2 protein where it is now confined to the optic nerve head (ONH) and optic stalk (OS) (Fig. 1D-D"). We also verified live GFP expression in adult *Pax2*$^{GFP/+}$ eyes using multimodal imaging: scanning laser ophthalmoscopy, coupled with optic coherence tomography (OCT) (Fig. 1E). This corresponds to endogenous expression in the optic disc and astrocyte domains (Parrilla et al., 2009; Stanke et al., 2010); the latter associated with adult retinal vasculature (arrow in Fig 1E). We conclude that this *Pax2*^{GFP} reporter is a reliable short-term marker of the Pax2 lineage during eye development. Other *Pax2* mutations cause brain, renal and ocular defects and early postnatal death (Soofi et al., 2012; Torres et al., 1995; Torres et al., 1996). *Pax2*$^{GFP/GFP}$ embryos also have brain exencephaly (Fig. 2C) and bilateral ocular coloboma (arrows in Figs. 2C', 2D), with GFP fluorescence visible through the residual gap from failed fissure closure (Figs 2D, 2D'). We propagated this allele >10 generations by separately backcrossing to C57BL/6J and CD-1 mice, the latter for bigger litters and albino eyes. In both cases, there was a 25% ratio of *Pax2*$^{GFP/GFP}$

embryos from heterozygous parental matings, which had completely penetrant eye phenotypes (n = 104 mutants in 386 embryos from 33 litters). However, there was weaker penetrance of the brain exencephaly (62% in C57BL/6 mutants, 80% in CD-1 mutants), differing from 100% reported for *Pax2*$^{KO/KO}$ mice (Torres et al., 1996).

Next, we qualitatively and quantitatively evaluated endogenous *Pax2* mRNA expression in wild type, heterozygous and homozygous *Pax2*^{GFP} eyes (Fig. 3, Suppl Fig 1). At E13.5, *Pax2* mRNA is readily observed through in situ hybridization within the ONH, optic stalk, inner ear and hindbrain (arrow) of *Pax2*$^{GFP/+}$ embryos (Figs 3A,3A'). *Pax2*$^{GFP/GFP}$ eyes lack *Pax2* mRNA expression in the ONH and optic stalk (5 of 6 E13.5 embryos tested by in situ) (Figs. 3E,3E' and Suppl Fig1). To quantify *Pax2* transcript levels, we collected E11.5 eye total RNA and performed qPCR, to find a >95% loss of mRNA in *Pax2*$^{GFP/GFP}$ eyes (n=3/3; Suppl Fig 1B). We noted that a proportion of mutant embryos retained *Pax2* mRNA hindbrain expression (arrow in Fig 3E), which is consistent with reduced phenotypic penetrance. We also evaluated Pax2 protein, using a well validated, specific polyclonal antibody (Suppl Table 1). Antibody labeling of control and mutant cryosections showed the complete absence of Pax2 protein in E13.5 mutant eyes (n = 3/3; Figs 3B,3F), although not in the hindbrain (data not shown). EGFP and endogenous Pax2 protein domains were tightly correlated in *Pax2* heterozygotes (Fig 3B-3D,3G,3H), but Pax2$^{GFP/GFP}$ eyes always displayed an enlarged GFP domain surrounding the normal position of the retinal-ONH boundary (Fig 3H). We do not attribute the broader GFP domain to reporter perdurance, because the GFP mRNA pattern was identical (compare Figs 3G to 3H). Instead, derepressed EGFP expression is consistent with *Pax2* normally repressing its own transcription (Schwarz et al., 2000). Overall, we conclude that at the *Pax2*$^{GFP/GFP}$ allele represents a protein null for the eye.

Pax2$^{GFP/GFP}$ eyes have nasal-specific defects and coloboma

Then, we followed the progression of optic fissure closure from E11.5-E13.5 (Figs 4 and 5). We assayed the juxtaposition of two transcription factors, the retinal progenitor cell (RPC)-specific protein Vsx2/Chx10 (Liu et al., 1994) and Mitf. Mitf is expressed by neural crest-derived cells, and developing and mature melanocytes in the retinal pigmented epithelium (RPE) (Hemesath et al., 1994; Hodgkinson et al., 1993). In E11.5 *Pax2*$^{GFP/+}$ retinas, the normal boundary between RPCs (magenta) and RPE (green) is apparent, with the RPE monolayer curving around to the distal tip of the optic cup while the fissure is still open (Fig. 4A,A'). However, *Pax2*$^{GFP/GFP}$ littermate eyes showed truncated Vsx2 expression only in the nasal cup (Fig 4 E,E'). This was accompanied by an expanded Mitf domain, suggesting compromised retina – RPE compartment boundary formation. To verify the spatial specificity of this phenotype, we tested the marker *Foxg1* (*Forkhead Box G1;BF-1*) in E11.5 and E13.5 eyes (Hatini et al., 1994; Huh et al., 1999). Normally, Foxg1 is restricted to the nasal half of the optic cup, in both retinal and RPE cells (Fig 4B). E11.5 *Pax2*$^{GFP/GFP}$ eyes retained nasal-restriction but the Foxg1 domain was abnormally shaped ventrally, along with an apposition of optic fissure edges and excess mesenchymal cells (arrow Fig 4F). By E13.5 the Foxg1 nasal domain was more comparable between genotypes, yet the fissure remained open in *Pax2* mutants, and the nasal retinal tip was abnormally pointed towards the lens (Fig 4C,G). We confirmed incomplete fissure closure in *Pax2* deficient retinas also affected the

basement membrane, using the marker laminin (reviewed in Hohenester and Yurchenco, 2013). In E13.5 *Pax2*$^{GFP/+}$ controls laminin is continuously expressed along the ventral surface of the cup (Fig 4D), but is absent once ventral cells fuse and lose their basement membranes (Fig 4D). In *Pax2*$^{GFP/GFP}$ eyes laminin expression clearly persisted and continued to outline the ventral opening (Fig 4H, arrow).

Because Foxg1 expression is only abnormal in ventral *Pax2*$^{GFP/GFP}$ eyes, we checked the status of dorso-ventral patterning using three markers with dorsal (*Tbx5*) or ventral (*Vax2, Raldh3*) restricted optic cup expression (Suppl Fig 2) (Barbieri et al., 2002; Koshiba-Takeuchi et al., 2000; Mic et al., 2000; Mui et al., 2002). All localized correctly (Suppl Fig 2), suggesting that *Pax2* is normally required for just nasal-temporal patterning, and consistent with *Pax2* acting epistatic to *Foxg1* (Smith et al., 2017). Abnormal expression of Vsx2, Mitf and Foxg1 in *Pax2* mutant eyes (Figs 4E-4E") suggests that the nasal optic cup may be more susceptible to retina-RPE cell fate changes that rely on *Pax2* activity (Baumer et al., 2003). This *en face*, sagittal view of *Pax2*$^{GFP/GFP}$ eyes does not fully depict this morphologic deformity, as perpendicular sections, along the horizontal plane, often had an abnormal fold only in the nasal cup (Figs 3F, 6E, Suppl Fig1). These cells expressed Foxg1, Pax6 and Vsx2 (not shown) identifying them as RPCs.

Past studies solidified an essential role for *Pax2* in establishing optic cup versus stalk territories (Schwarz et al., 2000). In E14.5 *Pax2*$^{-/-}$ eyes the transcription factors *Rax/Rx, Pax6* and *Mitf* were ectopically expressed in the optic stalk (Schwarz et al., 2000). Given the earlier mispatterning seen here for Vsx2 and Mitf (Fig 4F), we examined the retina versus RPE delineation in E13.5 eyes, along the horizontal section plane (Fig 5). Here we noted that Vsx2 is normally confined to RPCs and excluded from ONH cells (Figs 5A,5A'). While nuclear Mitf is present in RPE nuclei, it is also weakly expressed in the chevron-shaped ONH (Fig 5A,5A"). However, the Vsx2 domain was somewhat smaller, fuzzy and indistinct where the boundary with ONH should be in *Pax2*$^{GFP/GFP}$ eyes (Figs 5E,5E'). Mitf expression was abnormal too, extending uninterrupted into the optic stalk of *Pax2* mutants (Figs 5E,5E").

The early-acting transcription factor Rax was previously known to shift into the optic stalk of *Pax2*$^{-/-}$ eyes (Schwarz et al., 2000). Rax expression initiates in the anterior neural folds and eye field, with progressive restriction to embryonic retina by mid-gestation, and in the adult retina to Muller glia (Furukawa et al., 1997; Furukawa et al., 2000). Here we examined Rax protein expression, via a specific antibody, and directly compared it to Pax2^{GFP} expression. In E13.5 *Pax2*$^{GFP/+}$ eyes, Rax and GFP only overlap in the ONH (Fig 5B-B"), whereas in *Pax2*$^{GFP/GFP}$ eyes the broader Rax domain was coincident with that of Pax2^{GFP} (Fig 5F-F"). We also tested the bHLH factor Hes1, which has two simultaneous expression modes in the eye: oscillating in RPCs, but in the ONH high and sustained. We previously found that in *Hes1* retinal mutants the Pax6-Pax2 boundary is proximally shifted (Bosze et al., 2020). So, we asked whether high, sustained Hes1 is regulated by Pax2 (Figs 5C-C",5G-G"). We found that rather than a straight up or down level change, we could no longer discriminate between oscillatory versus high, sustained Hes1-expressing cells throughout the optic cup, ONH or optic stalk of *Pax2* mutants (Fig 5G). Finally, we tested *Vax1* expression (ventral anterior homeobox-1), which is localized to the ONH and optic stalk (Fig 5D)

(Bertuzzi et al., 1999; Hallonet et al., 1999). There was an inappropriate expansion of *Vax1* into the E13.5 mutant retina (Fig 5H). Taken together, we conclude that the *Pax2* mutant ONH retains molecular features of retina, RPE and ONH/OS cells, suggesting the normal ONH/OS developmental program stalls out, blocking neural-glial boundary formation.

Pax2 cross-regulation of Pax6

Early co-expression of Pax6 and Pax2 in the embryonic optic vesicle and cup, followed by their simultaneous mutual exclusion from the retina (Pax2) or optic stalk (Pax6) is one paradigm of tissue boundary formation. Although reciprocal suppression was previously demonstrated (Pax2 blocks *Pax6* in the optic stalk, while Pax6 suppresses *Pax2* in the retina) (Schwarz et al., 2000), there remain unanswered questions about these molecular mechanisms. Because we saw an expanded *Pax2* mutant lineage (GFP+cells) into the neural retina, we assume that *Pax2* autoregulation (repression) must also be one component of this process. Next, we took a deeper look at how Pax2 might normally block *Pax6* in the optic stalk. The *Pax6* gene has multiple promoters and is alternatively spliced, creating three major transcripts relevant to the mammalian eye: full-length Pax6 (FL), Pax6(5a) and paired-less Pax6 (Pax6Δ4PD) (Azuma et al., 2005; Carriere et al., 1993). *Pax6* also has a deeply-conserved intronic enhancer termed "α", which drives expression in a subset of retinal progenitor cells (Kammandel et al., 1999; Mui et al., 2005; Xu et al., 1999). Importantly, the α-enhancer has a validated Pax2 binding site located ~100bp upstream from the 5' start (P_α) of the Pax6ΔDPD transcript (Kammandel et al., 1999; Kim and Lauderdale, 2008; Lakowski et al., 2007). This prompted us to test whether *Pax2* selectively regulates the Pax6ΔPD isoform. First, we confirmed by in situ hybridization that *Pax6* mRNA is derepressed in $Pax2^{GFP/GFP}$ eyes (arrows in Figs 6A, 6E), phenocopying the $Pax2^{KO/KO}$ allele (Schwarz et al., 2000). However, our *Pax6* cRNA probe hybridizes to exons common to all three transcripts, so would be uninformative for selective changes in one particular isoform.

Two different strategies were used to test for *Pax2*-specific regulation of the Pax6ΔPD. The first takes advantage of validated Pax6 antibodies, one raised in rabbits against the C-terminus, common to both isoforms, and the other a monoclonal antibody specific for the paired-domain, thus recognizes only FL-Pax6 (Carriere et al., 1993; Kim and Lauderdale, 2008) (Suppl Table 1;Suppl Fig 3). Owing to their high specificity, these antibodies are reliable for co-labeling experiments (Suppl Fig 3). We triple antibody-labeled E13.5 control and *Pax2* mutant sections, including chick anti-GFP to visualize the $Pax2^{GFP}$ domain. We found that both FL-Pax6 and Pax6ΔPD proteins are ectopically expressed in the $Pax2^{GFP/GFP}$ optic stalk (arrows, Figs 6B-6D;6F-6H). The second experiment measured the relative molar ratios of these *Pax6* transcripts using triplex competitive RT-PCR and cDNA templates from manually-dissected GFP+ tissue from E13.5 $Pax2^{GFP/+}$ and $Pax2^{GFP/GFP}$ eyes (Figs 6I-6J). If one *Pax6* transcript is selectively derepressed when *Pax2* is removed, the ratios of Pax6FL to Pax6ΔPD would be shifted. Yet, there was no significant difference between genotypes (Fig 6K, $p = 0.054$), thus our data do not support selective regulation of a particular *Pax6* isoform. This suggests that other, more complex mechanisms remain to be explored here. For example, the presence of additional Pax2 binding sites in other *Pax6* enhancers; a redundant trans-acting factor that binds to the a-enhancer, and/or global *Pax2*

regulation through the recruitment of epigenetic modifying complexes to the *Pax6* locus (Kammandel et al., 1999; Ranghini and Dressler, 2015; Xu et al., 1999).

Hyperproliferation, cell death, RGC axon misrouting in *Pax2*$^{GFP/GFP}$ eyes

There have been no studies linking *Pax2* activity to cell proliferation in the eye. Yet the broader EGFP domain in *Pax2* mutants (Figs 3-8), prompted direct examination of this process. We quantified S-phase (EdU pulse-label incorporation) and M-phase (PHH3 expression) cells in E11.5 and E13.5 Pax2$^{GFP/+}$ and Pax2$^{GFP/GFP}$ sections (Figs 7A-D,7F-I). At E11.5 there was a significant increase in S-phase cells, but not for M-phase cells (Figs 7K,7L). But at E13.5, there was a loss of both S-and M-phase cells in the GFP-domain of *Pax2*$^{GFP/GFP}$ eyes, thereby defining a discrete developmental window when without *Pax2*, mitosis is deregulated. Next, we quantified the apoptotic marker cPARP in control and *Pax2* mutant eyes (Fig 7E,J). We found a significant increase in dying cells at E16.5 (Fig 7M), but not at younger stages (not shown). Interestingly many cPARP+ cells localized to the inner retina (arrow in Fig 7J). This is consistent with a downregulation of programmed cell death pathway genes in *no isthmus Pax2a* zebrafish mutants (Viringipurampeer et al., 2012).

The increased proliferation of E11.5 *Pax2* mutant cells and the larger GFP domain at E13.5, suggests that *Pax2* may normally orchestrate the tempo of cell division in ONH cells, relative to that of the adjacent retina. The loss of *Pax2* results in a larger ONH area, but does this occur at the expense of cells normally earmarked for neurogenesis? We tested this possibility in *Pax2*$^{GFP/+}$ and *Pax2*$^{GFP/GFP}$ sections that included the ONH/optic stalk, by co-labeling for GFP and the proneural bHLH factor Atoh7 (Figs 8A,8D). In *Pax2*$^{GFP/GFP}$ mutants, the Atoh7 domain appears shorter along the proximo-distal axis, yet wider on the apical-basal axis (Figs 8D,8D'). Moreover, the Atoh7 and GFP domains appear to overlap one another to a greater extent in *Pax2*$^{GFP/GFP}$ eyes. We also directly compared nascent RGC and their axons through anti-Tubb3 labeling (Figs 8B,8E), which also supports a misshapen retinal territory in mutant eyes. So we separately outlined and quantified the neurogenic (region with Atoh7+ cells) versus Pax2^{GFP} areas of the optic cup (Figs 8G', 8H, 8I). We saw that for both the nasal and temporal halves of the eye in *Pax2* mutants there was a significant increase in the ONH and loss of retinal area, although the wave of neurogenesis first begins on the temporal side (Hufnagel et al., 2010; Prada et al., 1991).

Anti-Tubb3 labeling also highlighted the RGC axon guidance defects in *Pax2* mutants, including invasion of the subretinal space (arrows in Fig 8E), as previously described (Torres et al., 1996). So, we tested *netrin1* mRNA expression, a classic RGC axon guidance cue normally localized to the ONH and optic stalk (Deiner et al., 1997). The *netrin1* mRNA domain was broader and more diffuse in *Pax2*$^{GFP/GFP}$ eyes (Figs 8C,8F). We conclude that without *Pax2* there is early ventronasal mispatterning, with *Pax2* lineage cells failing to stop proliferating. This contributes to failed optic fissure closure and aberrant RGC axon guidance. The inability of RGCs to find their targets leads to death, along with a proportion of *Pax2* mutant ONH cells unable to select a fate.

DISCUSSION

Despite decades of genetic analyses, our understanding of how mammalian gene networks simultaneously orchestrate tissue patterning, morphogenetic cell movements, growth, specification and differentiation is far from complete. In the eye, this process begins as the optic vesicle is regionalized via a molecular roadmap of proximodistal (P-D), dorsoventral (D-V), nasotemporal (N-T) and rostrocaudal (R-C) information. As the distal optic vesicle changes shape into a cup, two tissues, the RPE and neural retina appear, distinguishable from the proximal optic stalk. The borders between these tissues are delineated by the mutually exclusive expression of *Vsx2* and *Mitf* (retina versus RPE), or *Pax6* and *Pax2* (retina versus stalk). But in the past 20 years, there have been few new insights into how the cup-stalk interface is established or maintained. Here we used a $Pax2^{GFP}$ knock-in mouse to examine this very issue. Like other mutant alleles, $Pax2^{GFP/GFP}$ eyes have retinal and RPE marker expansion into the optic stalk (Schwarz et al., 2000), but we also discovered that ONH/OS genes like *Vax1* and *netrin1* inappropriately spread into retinal territory. Despite ventral restriction of *Pax2* to the E11.5 optic cup, it is also required during N-T patterning, and progenitor cell proliferation. Intriguingly, *Pax2* suppressed mitosis for only a short developmental period.

Pax2 in the early eye gene hierarchy

Early, uniform *Pax2* expression in the eye field and nascent optic vesicle (Nornes et al., 1990) is governed by both signaling pathways and CNS regionalizing transcription factors (Cai et al., 2013; Macdonald et al., 1995; Morcillo et al., 2006; Mui et al., 2005). Shh signaling from the ventral neural tube, in opposition to dorsal Bmp4, establishes the D-V axis, which in the eye activates *Pax2* (Cardozo et al., 2020; Macdonald et al., 1995). One striking demonstration that *Pax2* depends on Shh activity is the induction of a larger Pax2 domain and optic stalk upon global *Shh* mRNA overexpression in zebrafish embryos (Ekker et al., 1995; Gordon et al., 2018). *Pax2* is also regulated by *Vax* genes, since in the absence of *Vax1/2*, Shh induces, but does not maintain, *Pax2* expression (Mui et al., 2005). The subsequent restriction of *Pax2* to the ventral E10.5 optic cup (Nornes et al., 1990), implies that it might also act during D-V patterning. However, this patterning axis was normal in *Pax2* mutant eyes, with only ventronasal cells specifically requiring *Pax2*.

The optic vesicle/cup N-T axis is determined through *Shh* and *Fgf* signaling pathway interactions (Hernandez-Bejarano et al., 2015). One readout of these activities is the abutting expression of *Foxg1* and *Foxd1* in the nasal and temporal halves of the eye, respectively. *Foxg1* mutant mice have dysmorphic nasal optic cups, develop coloboma and RGC axon tracts that erroneously project ipsilaterally (Tian et al., 2008). This is consistent with prior descriptions of RGC axon guidance defects in $Pax2^{-/-}$ eyes (Torres et al., 1996). Interestingly, FoxG1 simultaneously blocks *Wnt8b*, but stimulates *Pax2* expression, prior to retinal neurogenesis (Smith et al., 2017). During zebrafish ocular morphogenesis, cells that line both sides of the choroid fissure derive from neighboring optic vesicle cells, which subsequently migrate via distinct routes to their final positions (Gordon et al., 2018). In *Pax2* mutant mice, we uncovered a nasal-specific morphologic deformity, which could also be the result of migration defects during ocular morphogenesis. After retinal, RPE, ONH and optic

stalk territories are established, *Pax2* activity remains essential for optic fissure closure and glial fate specification (Soukkarieh et al., 2007; Torres et al., 1996). Interestingly, we found abnormally large *Vax1* and *netrin1* domains, in $Pax2^{GFP/GFP}$ eyes extending into the neural retina, just like $Pax2^{GFP}$ expression. There was also a failure to distinguish salt-and-pepper (oscillating) from sustained Hes1-expressing cells, consistent with the idea that without *Pax2*, proximal optic cup and stalk cells fail to adopt a definitive tissue or cell identity.

Pax2 is an integral component of CNS compartment boundaries

How are tissue and cell lineage boundaries formed and maintained? The best-studied boundary in the developing CNS is rhombencephalic isthmus, which separates the embryonic midbrain from the hindbrain (Brand et al., 1996; Gibbs et al., 2017; Nakamura et al., 2005). Isthmus boundary cells proliferate at a slower rate, give rise to glial fates, and dictate aspects of neuronal specification in neighboring compartments (Kiecker and Lumsden, 2005). The position of the isthmus depends on a mutually repressive interaction between the *Otx2* and *Gbx2* transcription factors (Millet et al., 1999), but is further fine-tuned by multiple signals. Interestingly, *Pax2* is specifically expressed in the isthmus, with mutant embryos exhibiting brain exencephaly or malformation of the midbrain, isthmus and hindbrain (Brand et al., 1996; Schwarz et al., 1999; Schwarz et al., 1997). It has been suggested that the *Pax2* gene is a molecular hub that receives and integrates signaling inputs (reviewed in ALSomiry et al., 2019). For the eye ONH, this is an attractive idea, since Shh, Wnt, Bmp, Fgf and Retinoic acid signaling pathways are all active during ocular patterning, choroid fissure closure and RGC axon routing (reviewed in Cardozo et al., 2020). Yet, no *Pax2* ONH/optic stalk enhancer has been identified. Although a Pax6 consensus binding site in *Pax2* 5' noncoding DNA was tested *in vitro*, those assays lacked retinal context, hence also support Pax6 suppression of *Pax2* in the brain (Baumer et al., 2003; Schwarz et al., 2000). Indeed, multiple *Pax2* BAC transgenic mouse lines containing this Pax6 binding site display no optic vesicle, cup, ONH or OS expression (O'Sullivan et al., 2017; Ohyama and Groves, 2004). Thus, formal demonstration that *Pax2* is a signal integrator for the ONH must await discovery and characterization of its ONH/optic stalk enhancer(s).

It was already known that retinal and RPE markers spread down the optic stalk of *Pax2* mutants inappropriately. Conversely, loss of *Pax6* blocks retina and RPE formation, although some Pax2-expressing cells resembling the optic stalk persist (Baumer et al., 2003; Schwarz et al., 2000). This was interpreted that the ONH constrains retinal/RPE cells to the cup. Here we show the simultaneous presence of retinal, RPE and ONH/optic stalk markers in the *Pax2* mutant ONH lineage. Therefore, this region is initially multipotent, but kept on course to produce only glial fates. One characteristic of CNS boundary cells is slower progression through cell division (reviewed in Nakamura et al., 2005). At the brain isthmus high, sustained Hes1 expression is indicative of this deliberate pace, contrasting with oscillating Hes1 in adjacent, faster dividing neuronal progenitors (Baek et al., 2006; Imayoshi et al., 2013). In the eye, the ONH also requires high, sustained Hes1 expression (Bosze et al., 2020), which was not discernible in $Pax2^{GFP/GFP}$ eyes. We propose that *Pax2* maintains high Hes1 expression and the slower division rate. Interestingly, we found that $Pax2^{GFP/GFP}$ cells overproliferated for a relatively brief window of 48 hours, as neurogenesis normally initiates. Because *Hes1* mRNA and protein are initially uniform throughout the optic vesicle

and cup (Bosze et al., 2020; Lee et al., 2005), it is plausible that *Pax2* autonomously suppresses cells from converting to the faster division rate. However, since this is a dynamic process, only live imaging of embryonic mouse eyes can fully validate this idea.

In the developing kidney, *Pax2* maintains a lineage boundary between nephron and renal interstitial cells, by promoting nephrogenic fate (Davies, 2017; Naiman et al., 2017). *Pax2* null cells acquire the hybrid status of both nephron and interstitium progenitor cells, eventually differentiating erroneously as an interstitial cell (Naiman et al., 2017). By virtue of its ability to recruit epigenetic modifiers of gene expression and chromatin structure, *Pax2* keeps its kidney lineage on a particular developmental path. We found that in the eye, *Pax2* mutant ONH cells are also unable to maintain their normal course. This was evident from an inability to shut off retinal or RPE potential, maintain sustained Hes1 expression, and presumably eventually adopt the wrong fate. Because *Pax2* mutants die prenatally, the latter idea will need to be tested by selectively removing *Pax2* from the ONH/OS, then performing bulk and single cell analyses of the $Pax2^{GFP}$ populations. This will allow for extensive correlation of gene expression, mitotic status and open/closed chromatin configurations for the Pax2 lineage across the stage of ONH formation.

MATERIALS AND METHODS

Animals

$Pax2^{GFP/+}$ mice ($Pax2^{tm1.1Gdr}$) were maintained on both CD-1 and C57BL/6J backgrounds, genotyped using published primers (Soofi et al., 2012) and modified PCR conditions (35 cycles of 94°C X 30 sec, 53°C X 60 sec, 72°C X 60 sec). The genomic DNA integration sites for this $Pax2^{GFP}$ allele were validated by direct Sanger sequencing of PCR products from CD-1 mutant embryo genomic DNA. $Pax6^{Sey/+}$ mice ($Pax6^{Sey\text{-}Neu}$) were maintained on a FVB/N background and genotyped as described (Brown et al., 1998). α-Cre transgenic (Tg(Pax6-cre,GFP)2Pgr and $Pax6^{CKO/CKO}$ mice ($Pax6^{tm2pgr}$) were maintained on a CD-1 background and genotyped as described (Marquardt et al., 2001). The date of vaginal plug observation was assigned the age of E0.5. All mice were housed and cared for in accordance with guidelines provided by the National Institutes of Health, Bethesda, Maryland and the Association for Research in Vision and Ophthalmology, and conducted with approval and oversight from the UC Davis Institutional Animal Care and Use Committees.

OCT/SLO imaging

Adult $Pax2^{GFP/+}$ mice were live-imaged using a custom-built multimodal SLO-OCT system to visualize GFP+ cells with retinal tissue context (Zawadzki et al., 2015). Anesthetized mice were positioned on a heated custom stage. Mouse pupils were dilated, and the corneal surface prepared for custom contact lens application (Unicon Corporation). Imaging typically lasted 10-30 minutes with mice immediately returned to their cage and fully ambulatory in 10 minutes. Image processing used the Fiji version of Image J and MatLab (Miller et al., 2019; Zhang et al., 2015).

Immunohistochemistry

Embryos or embryonic heads were fixed in 4% paraformaldehyde/PBS for 1 hour on ice, processed by stepwise sucrose/PBS incubation ranging from 5-15%, and embedded in Tissue-Tek OCT, and 10μm cryosections generated. Antibody labeling was performed as in (Mastick and Andrews, 2001). The validated primary and secondary antibodies used are listed in Suppl Table 1. Nuclei were counterstained with DAPI (Sigma) or TOTO-3 iodide (Molecular Probes).

RNA *in situ* hybridization

DIG-labeled antisense riboprobes were synthesized from cDNA templates for GFP (gift from Nicholas Marsh-Armstrong), mouse Raldh3 (Li et al., 2000), mouse netrin1 (Kim et al., 2014), mouse Pax6 (Brown et al., 1998); mouse Pax2 (RRID:Addgene_13960), mouse Vax1(Bertuzzi et al., 1999), and mouse Vax2 (Dharmacon, 40101824). In situ probe labeling, cryosection hybridizations and color development used published protocols (Brown et al., 1998; Scholpp et al., 2003).

EdU incorporation

EdU pulse labeling was performed by injecting EdU in pregnant dams carrying E11.5 or E13.5 litters (12 μg/g body weight of 1mg/mL EdU in 0.15M NaCl) and harvesting embryos after 1.5 hours. EdU was detected using Click-iT EdU Cell Proliferation Kit for Imaging (Thermo Fisher Scientific Cat Number C10339).

Microscopy and Statistical analysis

Digital TIFF images of living GFP+ embryos were captured on a Leica MZ12 dissecting microscope, equipped with a UV light source, Spot B&W and color cameras and Spot software (v5.2). H&E stained or *in situ* hybridized sections were imaged with a Zeiss Axio Imager M.2 microscope, color camera and ZEN software (v2.6). Antibody-labeled cryosections were imaged using either a Leica DM5500 microscope, equipped with a SPEII solid state confocal and Leica LASX (v.3) software, or a Zeiss LSM-510 confocal microscope system and ZEN (v1) software. Post-image processing used ImageJ/FIJI Software (NIH) and Adobe Photoshop (CS5) programs to equivalently adjust for brightness, contrast, and pseudo-coloring. For all embryonic sections and cell counting, ≥3 individuals were analyzed, using at least 2 sections per individual. Sections were judged to be of equivalent depth by presence of or proximity to the optic nerve. Marker+ cells in tissue sections were counted using the count tool in Adobe Photoshop CS5 and statistical analyses performed with Prism GraphPad (v8) or Excel (v16.16.11) software, with p-values determined with t-test and a Welsh post-hoc test.

Triplex RT-PCR

E13.5 embryonic eyes were collected from $Pax2^{GFP/+X}$ $Pax2^{GFP/+}$ litters, the GFP+ domain hand-dissected, and tissues from each embryo pooled and snap frozen (n=3 biologic replicates/genotype). After PCR genotyping, total RNA was extracted (Zymo Research, Irvine, CA) and 50ng used for cDNA synthesis (iScript, BioRad, Hercules, CA). PCR reactions included 2.5 ng of each cDNA template, 1X Taq polymerase (Roche/Sigma), and

1X MasterAmp PCR additive (Lucigen, Middleton, WI), plus three oligonucleotide primers: an untagged 5' primer spanning the *Pax6* Exon3/4 splice junction (5'UTR FL); another untagged 5' primer situated in Intron 5 (5'UTR ΔPD); plus the shared 3' primer, within Exon5, end-labeled with 6-carboxyfluoroscein (FAM) (Fig 6; Suppl. Table 2). As internal controls for *Pax6* gene amplification, a primer pair specific to Exon 8 (common to both isoforms) was included in each assay (not shown). The resulting amplicons from 35 cycles of PCR (94°C X 30 sec, 60°C X 30 sec, 72°C X 30 sec) were denatured, and resolved by capillary electrophoresis (ABI 3130XL, Applied Biosystems, Waltham, MA), using the internal ROX-500 DNA size ladder. Peak areas reflect the molar abundance of full length *Pax6* (FL) versus pairedless *Pax6* (ΔPD) mRNA. Peak areas were determined using Peak Scanner 2.0 software (Thermo Fisher, Waltham, MA).

Quantitative RT-PCR

E11.5 optic cups from $Pax2^{GFP/+}$X $Pax2^{GFP/+}$ litters were collected by hand dissection and snap frozen as eye pairs while embryos were genotyped. Total RNA was extracted (Zymo Research, Irvine, CA) and 50ng used as template for cDNA synthesis (iScript, BioRad, Hercules, CA). *Pax2* transcripts were quantified by real-time quantitative PCR (StepOne Plus and Fast Sybr Green Master Mix, ABI). These values were normalized to the mean of *GAPDH* and *b-actin* mRNA levels (all primers are in Suppl. Table 2). The comparative CT method was used to compare samples to mRNA levels in wild type optic cups, which were assigned the value of 1 (Livak and Schmittgen, 2001).

Supplementary Material

Refer to Web version on PubMed Central for supplementary material.

Acknowledgements:

This work was supported by the NIH/NEI EY13612 grant to NLB; NIH/NEI Core Facilities grant P30 EY012576 to UC Davis; Society for Developmental Biology Choose Development! Fellowship to JS-N; the Children's Glaucoma Foundation, Vision for Tomorrow and University of Georgia, Dept. of Cellular Biology Vision Research Fund to JDL; and NIH/DDK grant DK054740 to GRD. The authors thank Ruth Ashery Padan for alpha-Cre and *Pax6* flox mice; Grant Mastick for *netrin1* cDNA; Nick Marsh-Armstrong for eGFP cDNA; Kapil Bharti for *Vax1* cDNA; Tom Glaser for *Raldh3* cDNA and *Pax6* triplex PCR advice; Ratheesh Kumar Meleppat and Robert Zawadzki for help with OCT/SLO imaging; Amy Riesenberg and April Bird for technical support, and the UC Davis Eye Development group for insightful discussions. We also thank Anna La Torre and Nick Marsh-Armstrong for critical evaluation of this manuscript.

References

ALSomiry AS, Gregory-Evans CY, Gregory-Evans K, 2019. An update on the genetics of ocular coloboma. Hum Genet 138, 865–880. [PubMed: 31073883]

Amiel J, Audollent S, Joly D, Dureau P, Salomon R, Tellier AL, Auge J, Bouissou F, Antignac C, Gubler MC, Eccles MR, Munnich A, Vekemans M, Lyonnet S, Attie-Bitach T, 2000. PAX2 mutations in renal-coloboma syndrome: mutational hotspot and germline mosaicism. Eur J Hum Genet 8, 820–826. [PubMed: 11093271]

Azuma N, Tadokoro K, Asaka A, Yamada M, Yamaguchi Y, Handa H, Matsushima S, Watanabe T, Kohsaka S, Kida Y, Shiraishi T, Ogura T, Shimamura K, Nakafuku M, 2005. The Pax6 isoform bearing an alternative spliced exon promotes the development of the neural retinal structure. Hum Mol Genet 14, 735–745. [PubMed: 15677484]

Baek JH, Hatakeyama J, Sakamoto S, Ohtsuka T, Kageyama R, 2006. Persistent and high levels of Hes1 expression regulate boundary formation in the developing central nervous system. Development 133, 2467–2476. [PubMed: 16728479]

Barbieri AM, Broccoli V, Bovolenta P, Alfano G, Marchitiello A, Mocchetti C, Crippa L, Bulfone A, Marigo V, Ballabio A, Banfi S, 2002. Vax2 inactivation in mouse determines alteration of the eye dorsal-ventral axis, misrouting of the optic fibres and eye coloboma. Development 129, 805–813. [PubMed: 11830579]

Baumer N, Marquardt T, Stoykova A, Spieler D, Treichel D, Ashery-Padan R, Gruss P, 2003. Retinal pigmented epithelium determination requires the redundant activities of Pax2 and Pax6. Development 130, 2903–2915. [PubMed: 12756174]

Bertuzzi S, Hindges R, Mui SH, O'Leary DD, Lemke G, 1999. The homeodomain protein vax1 is required for axon guidance and major tract formation in the developing forebrain. Genes Dev 13, 3092–3105. [PubMed: 10601035]

Blake JA, Ziman MR, 2014. Pax genes: regulators of lineage specification and progenitor cell maintenance. Development 141, 737–751. [PubMed: 24496612]

Bopp D, Burri M, Baumgartner S, Frigerio G, Noll M, 1986. Conservation of a large protein domain in the segmentation gene paired and in functionally related genes of Drosophila. Cell 47, 1033–1040. [PubMed: 2877747]

Bosze B, Moon MS, Kageyama R, Brown NL, 2020. Simultaneous Requirements for Hes1 in Retinal Neurogenesis and Optic Cup-Stalk Boundary Maintenance. J Neurosci 40, 1501–1513. [PubMed: 31949107]

Brand M, Heisenberg CP, Jiang YJ, Beuchle D, Lun K, Furutani-Seiki M, Granato M, Haffter P, Hammerschmidt M, Kane DA, Kelsh RN, Mullins MC, Odenthal J, van Eeden FJ, Nusslein-Volhard C, 1996. Mutations in zebrafish genes affecting the formation of the boundary between midbrain and hindbrain. Development 123, 179–190. [PubMed: 9007239]

Brown NL, Kanekar S, Vetter ML, Tucker PK, Gemza DL, Glaser T, 1998. Math5 encodes a murine basic helix-loop-helix transcription factor expressed during early stages of retinal neurogenesis. Development 125, 4821–4833. [PubMed: 9806930]

Cai Z, Tao C, Li H, Ladher R, Gotoh N, Feng GS, Wang F, Zhang X, 2013. Deficient FGF signaling causes optic nerve dysgenesis and ocular coloboma. Development 140, 2711–2723. [PubMed: 23720040]

Cardozo MJ, Almuedo-Castillo M, Bovlenta P, 2020. Patterning the Vertebrate Retina with Morphogenetic Signaling Pathways. The Neuroscientist 26, 185–196. [PubMed: 31509088]

Carriere C, Plaza S, Martin P, Quatannens B, Bailly M, Stehelin D, Saule S, 1993. Characterization of quail Pax-6 (Pax-QNR) proteins expressed in the neuroretina. Mol Cell Biol 13, 7257–7266. [PubMed: 8246948]

Cross SH, McKie L, West K, Coghill EL, Favor J, Bhattacharya S, Brown SD, Jackson IJ, 2011. The Opdc missense mutation of Pax2 has a milder than loss-of-function phenotype. Hum Mol Genet 20, 223–234. [PubMed: 20943750]

Davies J, 2017. Pax2: A "Keep to the Path" Sign on Waddington's Epigenetic Landscape. Dev Cell 41, 331–332. [PubMed: 28535367]

Deiner MS, Kennedy TE, Fazeli A, Serafini T, Tessier-Lavigne M, Sretavan DW, 1997. Netrin-1 and DCC mediate axon guidance locally at the optic disc: loss of function leads to optic nerve hypoplasia. Neuron 19, 575–589. [PubMed: 9331350]

Ekker SC, Ungar AR, Greenstein P, von Kessler DP, Porter JA, Moon RT, Beachy PA, 1995. Patterning activities of vertebrate hedgehog proteins in the developing eye and brain. Curr Biol 5, 944–955. [PubMed: 7583153]

Favor J, Sandulache R, Neuhauser-Klaus A, Pretsch W, Chatterjee B, Senft E, Wurst W, Blanquet V, Grimes P, Sporle R, Schughart K, 1996. The mouse Pax2(1Neu) mutation is identical to a human PAX2 mutation in a family with renal-coloboma syndrome and results in developmental defects of the brain, ear, eye, and kidney. Proc Natl Acad Sci U S A 93, 13870–13875. [PubMed: 8943028]

Fu W, Noll M, 1997. The Pax2 homolog sparkling is required for development of cone and pigment cells in the Drosophila eye. Genes Dev 11, 2066–2078. [PubMed: 9284046]

Fuhrmann S, 2010. Eye morphogenesis and patterning of the optic vesicle. Curr Top Dev Biol 93, 61–84. [PubMed: 20959163]

Furukawa T, Kozak CA, Cepko CL, 1997. rax, a novel paired-type homeobox gene, shows expression in the anterior neural fold and developing retina. Proc Natl Acad Sci U S A 94, 3088–3093. [PubMed: 9096350]

Furukawa T, Mukherjee S, Bao ZZ, Morrow EM, Cepko CL, 2000. rax, Hes1, and notch1 promote the formation of Muller glia by postnatal retinal progenitor cells. Neuron 26, 383–394. [PubMed: 10839357]

Gibbs HC, Chang-Gonzalez A, Hwang W, Yeh AT, Lekven AC, 2017. Midbrain-Hindbrain Boundary Morphogenesis: At the Intersection of Wnt and Fgf Signaling. Front Neuroanat 11, 64. [PubMed: 28824384]

Gordon HB, Lusk S, Carney KR, Wirick EO, Murray BF, Kwan KM, 2018. Hedgehog signaling regulates cell motility and optic fissure and stalk formation during vertebrate eye morphogenesis. Development 145.

Hallonet M, Hollemann T, Pieler T, Gruss P, 1999. Vax1, a novel homeobox-containing gene, directs development of the basal forebrain and visual system. Genes Dev 13, 3106–3114. [PubMed: 10601036]

Hatini V, Tao W, Lai E, 1994. Expression of winged helix genes, BF-1 and BF-2, define adjacent domains within the developing forebrain and retina. J Neurobiol 25, 1293–1309. [PubMed: 7815060]

Hemesath TJ, Steingrimsson E, McGill G, Hansen MJ, Vaught J, Hodgkinson CA, Arnheiter H, Copeland NG, Jenkins NA, Fisher DE, 1994. microphthalmia, a critical factor in melanocyte development, defines a discrete transcription factor family. Genes Dev 8, 2770–2780. [PubMed: 7958932]

Hernandez-Bejarano M, Gestri G, Spawls L, Nieto-Lopez F, Picker A, Tada M, Brand M, Bovolenta P, Wilson SW, Cavodeassi F, 2015. Opposing Shh and Fgf signals initiate nasotemporal patterning of the zebrafish retina. Development 142, 3933–3942. [PubMed: 26428010]

Hodgkinson CA, Moore KJ, Nakayama A, Steingrimsson E, Copeland NG, Jenkins NA, Arnheiter H, 1993. Mutations at the mouse microphthalmia locus are associated with defects in a gene encoding a novel basic-helix-loop-helix-zipper protein. Cell 74, 395–404. [PubMed: 8343963]

Hohenester E, Yurchenco PD, 2013. Laminins in basement membrane assembly. Cell Adh Migr 7, 56–63. [PubMed: 23076216]

Hufnagel RB, Le TT, Riesenberg AL, Brown NL, 2010. Neurog2 controls the leading edge of neurogenesis in the mammalian retina. Dev Biol 340, 490–503. [PubMed: 20144606]

Huh S, Hatini V, Marcus RC, Li SC, Lai E, 1999. Dorsal-ventral patterning defects in the eye of BF-1-deficient mice associated with a restricted loss of shh expression. Dev Biol 211, 53–63. [PubMed: 10373304]

Imayoshi I, Isomura A, Harima Y, Kawaguchi K, Kori H, Miyachi H, Fujiwara T, Ishidate F, Kageyama R, 2013. Oscillatory control of factors determining multipotency and fate in mouse neural progenitors. Science 342, 1203–1208. [PubMed: 24179156]

Kammandel B, Chowdhury K, Stoykova A, Aparicio S, Brenner S, Gruss P, 1999. Distinct cisessential modules direct the time-space pattern of the Pax6 gene activity. Dev Biol 205, 79–97. [PubMed: 9882499]

Keller SA, Jones JM, Boyle A, Barrow LL, Killen PD, Green DG, Kapousta NV, Hitchcock PF, Swank RT, Meisler MH, 1994. Kidney and retinal defects (Krd), a transgene-induced mutation with a deletion of mouse chromosome 19 that includes the Pax2 locus. Genomics 23, 309–320. [PubMed: 7835879]

Kiecker C, Lumsden A, 2005. Compartments and their boundaries in vertebrate brain development. Nat Rev Neurosci 6, 553–564. [PubMed: 15959467]

Kim J, Lauderdale JD, 2006. Analysis of Pax6 expression using a BAC transgene reveals the presence of a paired-less isoform of Pax6 in the eye and olfactory bulb. Dev Biol 292, 486–505. [PubMed: 16464444]

Kim J, Lauderdale JD, 2008. Overexpression of pairedless Pax6 in the retina disrupts corneal development and affects lens cell survival. Dev Biol 313, 434–454. [PubMed: 18062951]

Kim M, Farmer WT, Bjorke B, McMahon SA, Fabre PJ, Charron F, Mastick GS, 2014. Pioneer midbrain longitudinal axons navigate using a balance of Netrin attraction and Slit repulsion. Neural Dev 9, 17. [PubMed: 25056828]

Koshiba-Takeuchi K, Takeuchi JK, Matsumoto K, Momose T, Uno K, Hoepker V, Ogura K, Takahashi N, Nakamura H, Yasuda K, Ogura T, 2000. Tbx5 and the retinotectum projection. Science 287, 134–137. [PubMed: 10615048]

Kozmik Z, 2005. Pax genes in eye development and evolution. Curr Opin Genet Dev 15, 430–438. [PubMed: 15950457]

Lakowski J, Majumder A, Lauderdale JD, 2007. Mechanisms controlling Pax6 isoform expression in the retina have been conserved between teleosts and mammals. Dev Biol 307, 498–520. [PubMed: 17509554]

Lee HY, Wroblewski E, Philips GT, Stair CN, Conley K, Reedy M, Mastick GS, Brown NL, 2005. Multiple requirements for Hes 1 during early eye formation. Dev Biol 284, 464–478. [PubMed: 16038893]

Li H, Wagner E, McCaffery P, Smith D, Andreadis A, Drager UC, 2000. A retinoic acid synthesizing enzyme in ventral retina and telencephalon of the embryonic mouse. Mech Dev 95, 283–289. [PubMed: 10906479]

Liu IS, Chen JD, Ploder L, Vidgen D, van der Kooy D, Kalnins VI, McInnes RR, 1994. Developmental expression of a novel murine homeobox gene (Chx10): evidence for roles in determination of the neuroretina and inner nuclear layer. Neuron 13, 377–393. [PubMed: 7914735]

Livak KJ, Schmittgen TD, 2001. Analysis of relative gene expression data using real-time quantitative PCR and the 2(-Delta Delta C(T)) Method. Methods 25, 402–408. [PubMed: 11846609]

Macdonald R, Barth KA, Xu Q, Holder N, Mikkola I, Wilson SW, 1995. Midline signalling is required for Pax gene regulation and patterning of the eyes. Development 121, 3267–3278. [PubMed: 7588061]

Marquardt T, Ashery-Padan R, Andrejewski N, Scardigli R, Guillemot F, Gruss P, 2001. Pax6 is required for the multipotent state of retinal progenitor cells. Cell 105, 43–55. [PubMed: 11301001]

Martinez-Morales JR, Cavodeassi F, Bovolenta P, 2017. Coordinated Morphogenetic Mechanisms Shape the Vertebrate Eye. Front Neurosci 11, 721. [PubMed: 29326547]

Mastick GS, Andrews GL, 2001. Pax6 regulates the identity of embryonic diencephalic neurons. Mol Cell Neurosci 17, 190–207. [PubMed: 11161479]

Mic FA, Molotkov A, Fan X, Cuenca AE, Duester G, 2000. RALDH3, a retinaldehyde dehydrogenase that generates retinoic acid, is expressed in the ventral retina, otic vesicle and olfactory pit during mouse development. Mech Dev 97, 227–230. [PubMed: 11025231]

Miller EB, Zhang P, Ching K, Pugh EN Jr., Burns ME, 2019. In vivo imaging reveals transient microglia recruitment and functional recovery of photoreceptor signaling after injury. Proc Natl Acad Sci U S A 116, 16603–16612. [PubMed: 31350349]

Millet S, Campbell K, Epstein DJ, Losos K, Harris E, Joyner AL, 1999. A role for Gbx2 in repression of Otx2 and positioning the mid/hindbrain organizer. Nature 401, 161–164. [PubMed: 10490024]

Morcillo J, Martinez-Morales JR, Trousse F, Fermin Y, Sowden JC, Bovolenta P, 2006. Proper patterning of the optic fissure requires the sequential activity of BMP7 and SHH. Development 133, 3179–3190. [PubMed: 16854970]

Mui SH, Hindges R, O'Leary DD, Lemke G, Bertuzzi S, 2002. The homeodomain protein Vax2 patterns the dorsoventral and nasotemporal axes of the eye. Development 129, 797–804. [PubMed: 11830578]

Mui SH, Kim JW, Lemke G, Bertuzzi S, 2005. Vax genes ventralize the embryonic eye. Genes Dev 19, 1249–1259. [PubMed: 15905411]

Naiman N, Fujioka K, Fujino M, Valerius MT, Potter SS, McMahon AP, Kobayashi A, 2017. Repression of Interstitial Identity in Nephron Progenitor Cells by Pax2 Establishes the Nephron-Interstitium Boundary during Kidney Development. Dev Cell 41, 349–365.e343. [PubMed: 28535371]

Nakamura H, Katahira T, Matsunaga E, Sato T, 2005. Isthmus organizer for midbrain and hindbrain development. Brain Research Reviews 49, 120–126. [PubMed: 16111543]

Nornes HO, Dressler GR, Knapik EW, Deutsch U, Gruss P, 1990. Spatially and temporally restricted expression of Pax2 during murine neurogenesis. Development 109, 797–809. [PubMed: 1977575]

O'Sullivan ML, Punal VM, Kerstein PC, Brzezinski J.A.t., Glaser T, Wright KM, Kay JN, 2017. Astrocytes follow ganglion cell axons to establish an angiogenic template during retinal development. Glia 65, 1697–1716. [PubMed: 28722174]

Ohyama T, Groves AK, 2004. Generation of Pax2-Cre mice by modification of a Pax2 bacterial artificial chromosome. Genesis 38, 195–199. [PubMed: 15083520]

Otteson DC, Shelden E, Jones JM, Kameoka J, Hitchcock PF, 1998. Pax2 expression and retinal morphogenesis in the normal and Krd mouse. Dev Biol 193, 209–224. [PubMed: 9473325]

Parrilla M, Lillo C, Herrero-Turrion MJ, Arevalo R, Lara JM, Aijon J, Velasco A, 2009. Pax2 in the optic nerve of the goldfish, a model of continuous growth. Brain Res 1255, 75–88. [PubMed: 19109934]

Prada C, Puga J, Perez-Mendez L, Lopez And R, Ramirez G, 1991. Spatial and Temporal Patterns of Neurogenesis in the Chick Retina. Eur J Neurosci 3, 1187. [PubMed: 12106248]

Prosser J, van Heyningen V, 1998. PAX6 mutations reviewed. Hum Mutat 11, 93–108. [PubMed: 9482572]

Ranghini EJ, Dressler GR, 2015. Evidence for intermediate mesoderm and kidney progenitor cell specification by Pax2 and PTIP dependent mechanisms. Dev Biol 399, 296–305. [PubMed: 25617721]

Sanyanusin P, Schimmenti LA, McNoe LA, Ward TA, Pierpont ME, Sullivan MJ, Dobyns WB, Eccles MR, 1995. Mutation of the PAX2 gene in a family with optic nerve colobomas, renal anomalies and vesicoureteral reflux. Nat Genet 9, 358–364. [PubMed: 7795640]

Schaefer SA, Higashi AY, Loomis B, Schrepfer T, Wan G, Corfas G, Dressler GR, Duncan RK, 2018. From Otic Induction to Hair Cell Production: Pax2(EGFP) Cell Line Illuminates Key Stages of Development in Mouse Inner Ear Organoid Model. Stem Cells Dev 27, 237–251. [PubMed: 29272992]

Scholpp S, Lohs C, Brand M, 2003. Engrailed and Fgf8 act synergistically to maintain the boundary between diencephalon and mesencephalon. Development 130, 4881–4893. [PubMed: 12917294]

Schwarz M, Alvarez-Bolado G, Dressler G, Urbanek P, Busslinger M, Gruss P, 1999. Pax2/5 and Pax6 subdivide the early neural tube into three domains. Mech Dev 82, 29–39. [PubMed: 10354469]

Schwarz M, Alvarez-Bolado G, Urbánek P, Busslinger M, Gruss P, 1997. Conserved biological function between Pax-2 and Pax-5 in midbrain and cerebellum development: evidence from targeted mutations. Proc Natl Acad Sci U S A 94, 14518–14523. [PubMed: 9405645]

Schwarz M, Cecconi F, Bernier G, Andrejewski N, Kammandel B, Wagner M, Gruss P, 2000. Spatial specification of mammalian eye territories by reciprocal transcriptional repression of Pax2 and Pax6. Development 127, 4325–4334. [PubMed: 11003833]

Shaham O, Menuchin Y, Farhy C, Ashery-Padan R, 2012. Pax6: a multi-level regulator of ocular development. Prog Retin Eye Res 31, 351–376. [PubMed: 22561546]

Sisodiya SM, Free SL, Williamson KA, Mitchell TN, Willis C, Stevens JM, Kendall BE, Shorvon SD, Hanson IM, Moore AT, van Heyningen V, 2001. PAX6 haploinsufficiency causes cerebral malformation and olfactory dysfunction in humans. Nat Genet 28, 214–216. [PubMed: 11431688]

Smith R, Huang YT, Tian T, Vojtasova D, Mesalles-Naranjo O, Pollard SM, Pratt T, Price DJ, Fotaki V, 2017. The Transcription Factor Foxg1 Promotes Optic Fissure Closure in the Mouse by Suppressing Wnt8b in the Nasal Optic Stalk. J Neurosci 37, 7975–7993. [PubMed: 28729440]

Soofi A, Levitan I, Dressler GR, 2012. Two novel EGFP insertion alleles reveal unique aspects of Pax2 function in embryonic and adult kidneys. Dev Biol 365, 241–250. [PubMed: 22410172]

Soukkarieh C, Agius E, Soula C, Cochard P, 2007. Pax2 regulates neuronal-glial cell fate choice in the embryonic optic nerve. Dev Biol 303, 800–813. [PubMed: 17173889]

Stanke J, Moose HE, El-Hodiri HM, Fischer AJ, 2010. Comparative study of Pax2 expression in glial cells in the retina and optic nerve of birds and mammals. J Comp Neurol 518, 2316–2333. [PubMed: 20437530]

Tao C, Zhang X, 2014. Development of astrocytes in the vertebrate eye. Dev Dyn 243, 1501–1510. [PubMed: 25236977]

Tian NM, Pratt T, Price DJ, 2008. Foxg1 regulates retinal axon pathfinding by repressing an ipsilateral program in nasal retina and by causing optic chiasm cells to exert a net axonal growth-promoting activity. Development 135, 4081–4089. [PubMed: 19004857]

Torres M, Gomez-Pardo E, Dressler GR, Gruss P, 1995. Pax-2 controls multiple steps of urogenital development. Development 121, 4057–4065. [PubMed: 8575306]

Torres M, Gomez-Pardo E, Gruss P, 1996. Pax2 contributes to inner ear patterning and optic nerve trajectory. Development 122, 3381–3391. [PubMed: 8951055]

Tzoulaki I, White IM, Hanson IM, 2005. PAX6 mutations: genotype-phenotype correlations. BMC Genet 6, 27. [PubMed: 15918896]

Viringipurampeer IA, Ferreira T, DeMaria S, Yoon JJ, Shan X, Moosajee M, Gregory-Evans K, Ngai J, Gregory-Evans CY, 2012. Pax2 regulates a fadd-dependent molecular switch that drives tissue fusion during eye development. Hum Mol Genet 21, 2357–2369. [PubMed: 22357656]

Xu PX, Zhang X, Heaney S, Yoon A, Michelson AM, Maas RL, 1999. Regulation of Pax6 expression is conserved between mice and flies. Development 126, 383–395. [PubMed: 9847251]

Zawadzki RJ, Zhang P, Zam A, Miller EB, Goswami M, Wang X, Jonnal RS, Lee SH, Kim DY, Flannery JG, Werner JS, Burns ME, Pugh EN Jr., 2015. Adaptive-optics SLO imaging combined with widefield OCT and SLO enables precise 3D localization of fluorescent cells in the mouse retina. Biomed Opt Express 6, 2191–2210. [PubMed: 26114038]

Zhang P, Zam A, Jian Y, Wang X, Li Y, Lam KS, Burns ME, Sarunic MV, Pugh EN Jr., Zawadzki RJ, 2015. In vivo wide-field multispectral scanning laser ophthalmoscopy-optical coherence tomography mouse retinal imager: longitudinal imaging of ganglion cells, microglia, and Muller glia, and mapping of the mouse retinal and choroidal vasculature. J Biomed Opt 20, 126005. [PubMed: 26677070]

Highlights:

- *Pax2*-GFP knock-in mutants show expansion of the developing optic nerve head territory
- *Pax2* is required for patterning the ventronasal optic cup
- *Pax2* is necessary for ocular progenitor cell proliferation within a discrete time window
- Optic nerve head cells are tripotential for retina, RPE or optic stalk fates

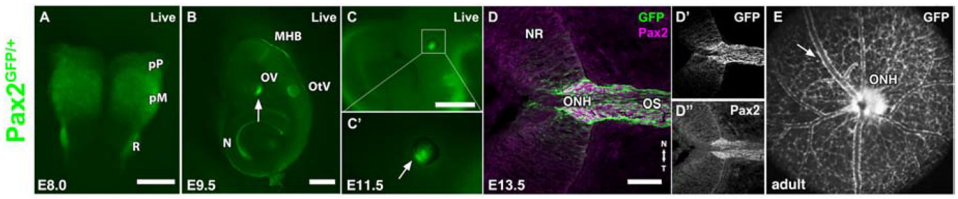

Figure 1. Comparison of *Pax2*^{GFP} and endogenous Pax2 ocular expression.

(A) At E8 EGFP fluorescence corresponds to known *Pax2* mRNA and protein domains (Nornes et al., 1990; Schwarz et al., 2000). (B) Live *Pax2*^{GFP} expression in the E9.5 optic cup, otic vesicle, midbrain-hindbrain boundary and the developing kidneys. (C,C') *Pax2*^{GFP} expression in E11.5 live embryos in the ventral optic cup (arrow in C'). (D-D") Antibody colabeling of E13.5 ocular sections shows overlap of GFP endogenous Pax2 proteins in the ONH. (E) SLO live image of 6 month old *Pax2*$^{GFP/+}$ eye fundus. Arrow points to a GFP+ retinal astrocyte. pP – presumptive prosencephalon, pM – presumptive mesencephalon, R – rhombencephalon; MHB – midbrain-hindbrain boundary; OV – optic vesicle; OtV – otic vesicle, N - nephros; NR = neural retina; ONH = optic nerve head; OS = optic stalk; Anterior is up in A; to left in B,C,C';nasal is up in D-D". Scalebar = 250μm in A;500 μm in B,C;50 μm in D.

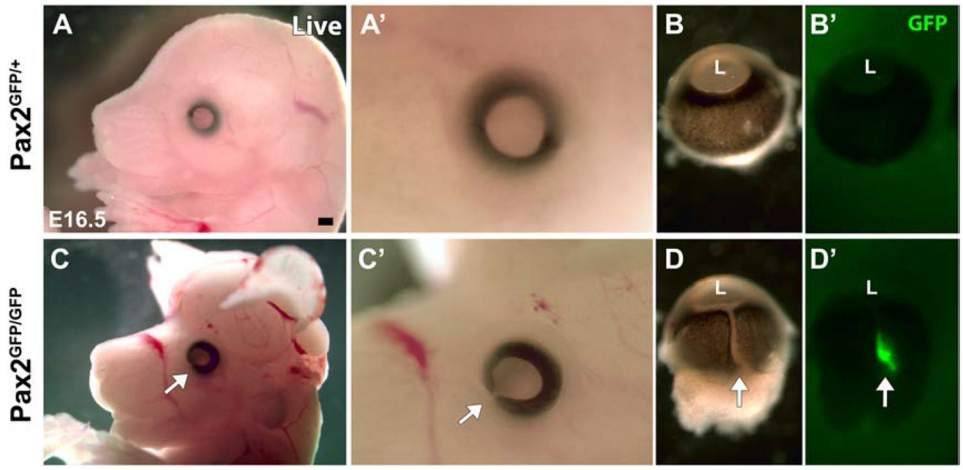

Figure 2. Brain and eye deformities of *Pax2*$^{GFP/GFP}$ embryos.

(A,A',C,C') Lateral views of E16.5 live embryos. *Pax2*$^{GFP/GFP}$ animals with exencephaly and ocular colobomas (arrow in C,C'). (B,B',D,D') The optic fissure remains open as a ventral cleft in *Pax2*$^{GFP/GFP}$ mutant eyes (arrow in D), with GFP fluorescence visible (arrow in D') (n=4/genotype). L – lens, Rostral is left in A,C; distal up in B,D. Scalebar = 500 μm

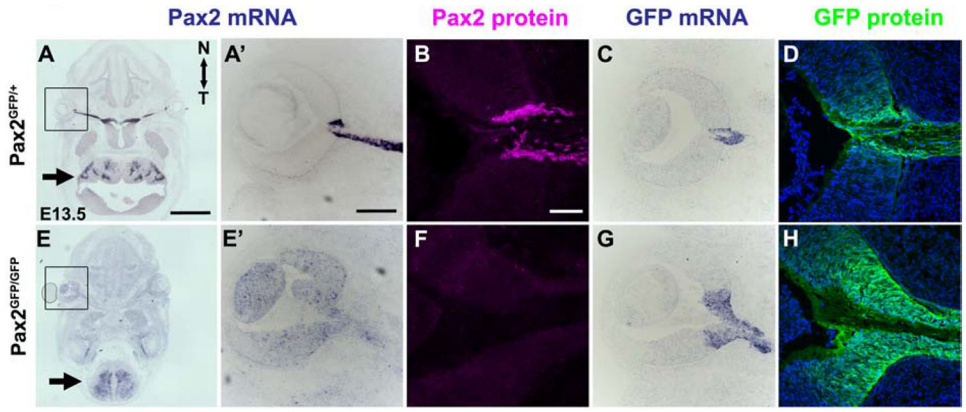

Figure 3. Downregulated *Pax2* mRNA but total loss of Pax2 protein in *Pax2*$^{GFP/GFP}$ eyes.

All panels have horizontal sections, with nasal up. (A,A',E,E') *Pax2* mRNA expression shown by in situ hybridization, with boxed areas shown at higher mag in A',E'. At E13.5, *Pax2* transcripts are normally visible in sections containing both eye and hindbrain (arrow) (A). E13.5 *Pax2*$^{GFP/GFP}$ sections contain residual *Pax2* mRNA in hindbrain (arrow), but loss of specific signal in the mutant ONH and OS (E, E'). This embryo had non-specific background (e.g., lens), but other embryos analyzed in parallel show near total loss of *Pax2* mRNA (Suppl Fig 1). (B, F) Anti-Pax2 labeling of E13.5 *Pax2*$^{GFf/+}$ and *Pax2*$^{GFP/GFP}$ sections demonstrate complete loss of Pax2 protein in the mutant ONH and optic stalk. (C,G) EGFP mRNA expression is expanded into retina in *Pax2*$^{GFP/GFP}$ eyes. (D,H) Anti-GFP labeling of sections nearby to C,G highlight expanded GFP protein domain in mutants (n=3 biologic replicates/genotype). Panels A,E are stitched composites of 9 image tiles. Scalebar: A =250 μm, A',B = 50 μm.

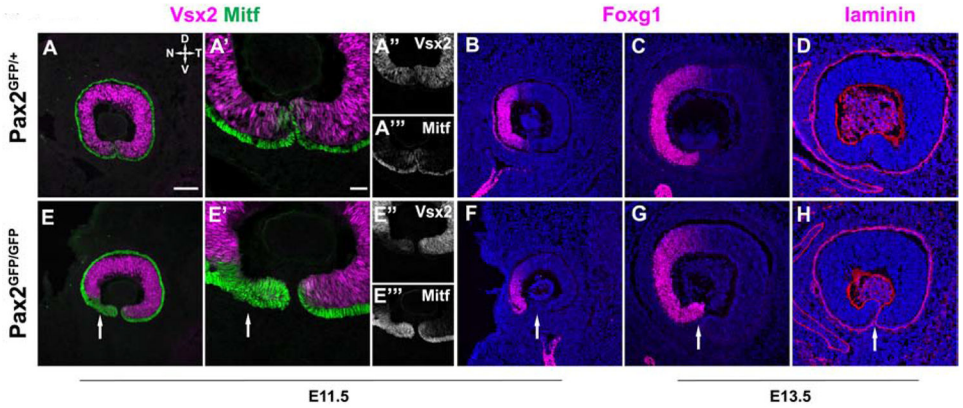

Figure 4. Nasotemporal and optic fissure defects of *Pax2*$^{GFP/GFP}$ mutants

All panels show sagittal view of eye. (A,A',F,F') Vsx2-Mitf colabeling of E11.5 sections. In the ventronasal optic, Mitf domain is expanded at the expense of Vsx2/Chx10. (B,F) At E11.5, Foxg1 immunostaining also highlights proportionally smaller nasal side of *Pax2*$^{GFP/GFP}$ optic cup. (C,G) In E13.5 *Pax2* mutants, optic cup size and the Foxg1 domain better resemble controls, but nasal tip is abnormally positioned, emphasizing failed fissure closure (D,H) E13.5 Anti-laminin labeling of the basement membrane also highlights failed fissure closure of *Pax2*$^{GFP/GFP}$ eyes (arrow in H). n = 3 biologic replicates/genotype Scalebar = 50μm

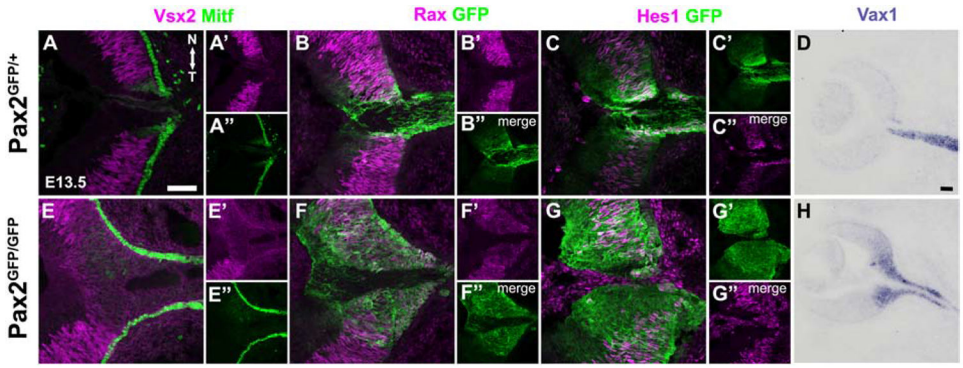

Figure 5. Abnormal marker expression in the ONH of *Pax2*$^{GFP/GFP}$ eyes

All panels oriented with rostral left and nasal up. (A,E) Vsx2 + Mitf colabeling normally highlights the retina-RPE boundary at E13.5, along with typical weak Mitf expression in ONH cells. *Pax2* mutants have a truncated Vsx2 domain, with the RPE extending continuously down the optic stalk. (B,F) By contrast, Rax expression is derepressed in the GFP+ domain *Pax2* mutant eyes (C,G) E13.5 Hes1+ GFP colabeling normally highlights higher, sustained Hes1 expression in the Pax2-GFP domain. The separation of these domains is no longer discernible in *Pax2*$^{GFP/GFP}$ eyes. (D,H) *Vax1* mRNA is normally confined to the ONH and OS at E13.5, but abnormally expanded into the optic cup of *Pax2*$^{GFP/GFP}$ eyes. n = 3 biologic replicates/genotype Scalebar = 50μm

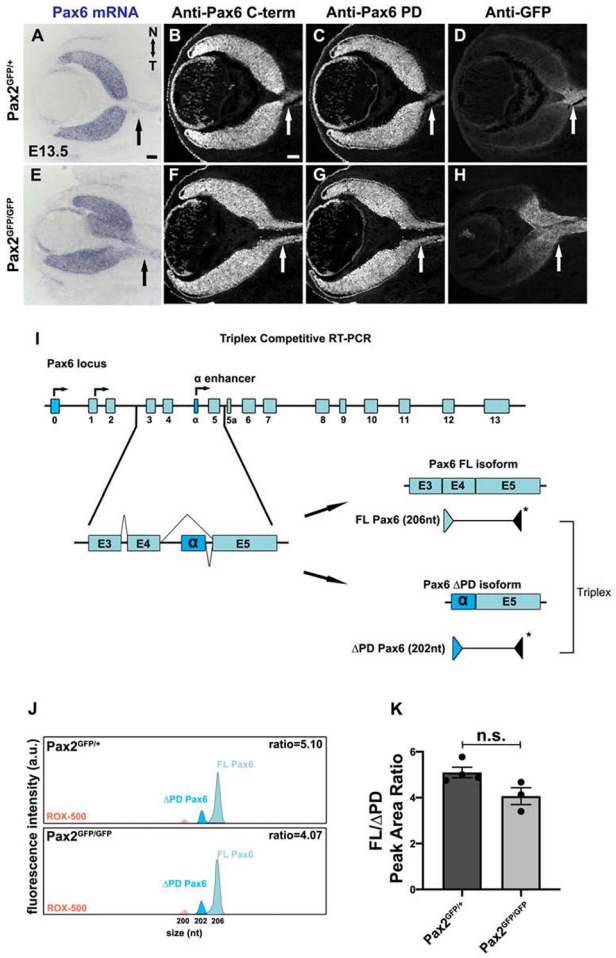

Figure 6. Coordinate derepression of *Pax6* isoforms in *Pax2* mutants

(A) In situ hybridization shows *Pax6* mRNA derepression into E13.5 ONH and optic stalk of $Pax2^{GFP/GFP}$ eyes. (B,F) Immunostaining using C-terminal polyclonal Pax6 antibody that recognizes multiple protein isoforms (FL + ΔPD, see Suppl Fig 3) also shows expanded expression into the optic stalk of $Pax2^{GFP/GFP}$ eyes (n=3/3 mutants) (C,G) Pax6 paired-domain specific antibody confirms FL Pax6 isoform derepression in *Pax2* mutants (n=3/3 mutants) (D,H) All B-G sections were colabeled with anti-GFP to confirm Pax6 isoforms spread into the $Pax2^{GFP}$ domain. (I) Triplex RT-PCR strategy to compare the relative abundance of *Pax6* mRNA isoforms in $Pax2^{GFP/+}$ and $Pax2^{GFP/GFP}$ eyes. The FAM labeled (*) 3 ’ primer resides in sequences common to both isoforms; while unlabeled 5’ primers are specific for the FL or ΔPD isoform. Competitive amplification of each product reflects isoform abundance. (J) Representative capillary electrophoresis profiles of PCR products from $Pax2^{GFP/+}$ and $Pax2^{GFP/GFP}$ cDNAs. The average ratio of FL (206nt) and ΔPD (202nt) cDNA peak areas reflect the relative abundance of each isoform. The 200nt peak (pink) is the ROX-500 size standard. (K) The average ratio of Pax6 FL/ΔPD cDNA peak areas plotted show no significant difference between $Pax2^{GFP/+}$ and $Pax2^{GFP/GFP}$ ONH domains (n = 3 biologic replicates/genotype; p=0.054). Graph displays individual replicate data points, mean and S.E.M. Scalebar = 50μm

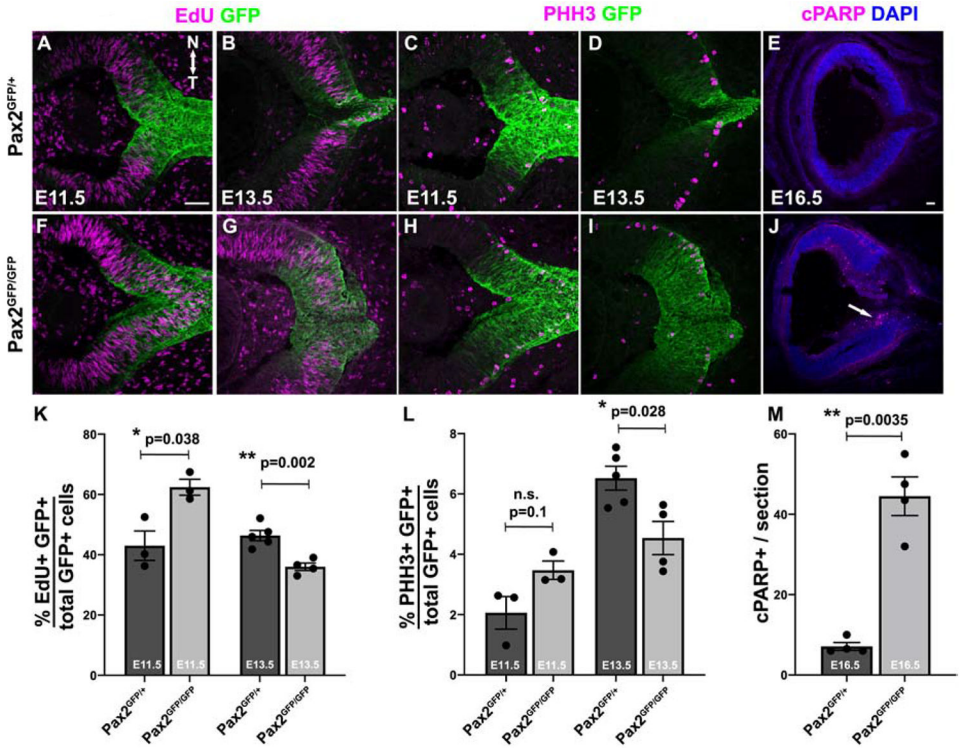

Figure 7. Early proliferation increase followed by apoptosis in the absence of *Pax2*

(A,B,F,G) E11.5 and E13.5 sections with the ONH/OS from EdU pulse-labeled embryos. (C,D,H,I) Anti PhosphoHistone-H3 (PHH3) M-phase cell labeling at E11.5 and E13.5 sections (E,J) Anti-cPARP labeling at E16.5 to assess apoptosis. (K-M) Quantification of S-Phase, M-Phase or apoptotic cells. K,L) Both EdU pulse labeling and PHH3 expression indicate overproliferation of GFP-labeled population in *Pax2*$^{GFP/GFP}$ eyes at E11.5, followed by a significant decline by E13.5 (K,L). At E16.5 the number of cPARP+ cells in *Pax2*$^{GFP/GFP}$ mutant sections was dramatically increased, many located in the nascent RGC inner layer (J). Graphs display individual replicate data points, the mean and S.E.M;* = $p<0.05$; ** = $p<0.01$; Scalebar in A,E = 50μm; n = ≥2 sections from 3 biologic replicates/ genotype.

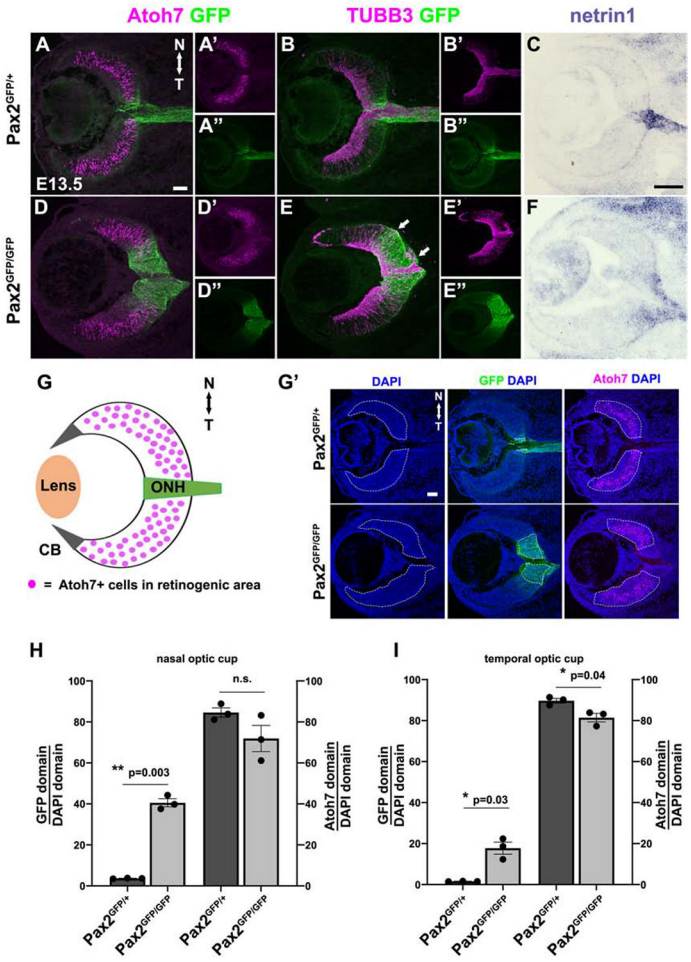

Figure 8. Loss of the neural-glial boundary impacts RGC axon guidance.

(A,D) Atoh7 and GFP colabeling of sections at the ONH/OS. In *Pax2* mutants, the Atoh7 domain relative to that of expanded GFP suggests a loss of retinal neurogenic territory with the nasal more affected (D, G). However, a proportion of *Pax2* mutant GFP+ cells remain Atoh7+. (B,E) TUBB3 + GFP colabeling is consistent with mutant GFP+ cells retaining neuronal characteristics, plus highlights RGC axon misrouting to the subretinal space (arrows). (C,F) *netrin1* mRNA ONH domain is more diffuse in $Pax2^{GFP/GFP}$ retina. (G) Atoh7 and $Pax2^{GFP}$ domain diagram. (G') The measured relative area of DAPI, $Pax2^{GFP}$ or Atoh7 image channels mark with white dotted lines for nasal and temporal cup. (H,I) Graphical depiction of increased GFP territory and smaller Atoh7+ territory on both sides of $Pax2^{GFP/GFP}$ eyes. Individual data points, the mean and S.E.M are shown;* = $p<0.05$; ** = $p<0.01$; Scalebar = 50μm; n = 3 biologic replicates per genotype.